Finite Element Mechanical Simulation of I-Section Post Composite Insulators

Tianfang Zhao [1,*], Yunpeng Liu [1], Le Li [1] and Songsong Zhou [2]

[1] Department of Electrical Engineering, North China Electric Power University, Baoding, China

[2] China Electric Power Research Institute, Beijing, China

* Corresponding Author Email: 1242772551@qq.com

Abstract. With the implementation of the "Carbon Neutrality and Carbon Peak" action plan, the demand for ultra-high voltage (UHV) insulation equipment in power systems has become increasingly urgent. Currently, the core diameter of ±800kV pillar composite insulators for UHV projects is mostly φ220mm or larger. However, from the perspective of material forming processes, "large dimensions" have always been a technical challenge. This paper shifts away from the traditional approach of solely focusing on overcoming large-diameter processing difficulties. Instead, it conducts a mechanical performance simulation of I-section pillar composite insulators. Under bending, and torsion conditions, the deformation of I-section pillar composite insulators is analyzed based on displacement and stress. The study aims to provide theoretical and practical support for the design and application of I-section pillar composite insulators.

Keywords: Ultra-High Voltage (UHV); I-section composite insulator; Mechanical performance; Finite element simulation.

1. Introduction

The design of I-section pillar composite insulators is a complex task due to the anisotropic nature of FRP materials. Unlike traditional materials such as steel, FRP requires careful consideration of reinforcement placement and layup patterns to achieve optimal mechanical performance. Previous studies in the construction field have demonstrated the effectiveness of I-section designs in steel structures. For instance, Fan et al. used ABAQUS to analyze the stress, load-bearing capacity, and deformation of I-section steel tubes by varying parameters such as the web-flange width ratio, width-to-thickness ratio, and height-to-width ratio [1-3]. Similarly, Deng et al. employed ANSYS to perform parametric modeling and optimization of double-symmetrical I-section beams, deriving the optimal cross-section that meets all design constraints with minimal computational effort [4-5].

However, the design of large FRP profiles cannot simply replicate these approaches due to the material's unique properties. The selection and arrangement of reinforcement materials must be tailored to the specific stress states of each section, ensuring efficient material usage and structural integrity [6-7]. This paper addresses these challenges by developing an I-section pillar composite insulator and conducting finite element simulations under compression, bending, and torsion conditions. The stress and displacement distributions are analyzed to evaluate the overall mechanical performance of the design.

2. Establishment of Solid Mechanics Simulation Model

The overall dimensions of the I-shaped core rod are 320mm (length) × 250mm (width), with a middle width of 50mm and transition curvature radii of 20mm and 60mm, as shown in Fig.1.

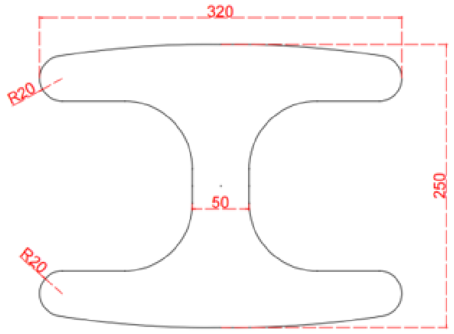

Fig 1. 320mm×250mm I-shaped cross-section.

The height of the core is based on the 5630mm height of the lower pillar of the ±800kV cylindrical post composite insulator (model ZGW6-816) produced by Henan Pinggao Electric Co., Ltd. The I-shaped core is formed by extrusion, as shown in Figure 2. For comparison with traditional post insulators, a cylindrical post composite insulator of the same height is also established, as shown in Figure 3.

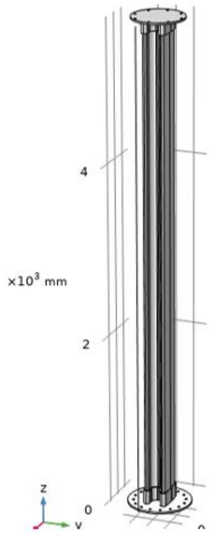

Fig 2. I-shaped post composite insulator with mounted flanges.

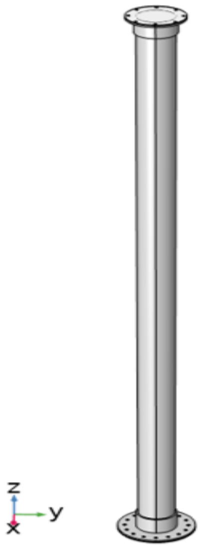

Fig 3. Cylindrical post composite insulator.

The upper and lower flanges of the ±800kV I-shaped cross-section are designed with reference to the ±800kV cylindrical post composite insulator (model ZGW6-816) produced by Henan Pinggao Electric Co., Ltd., as shown in Fig.4.

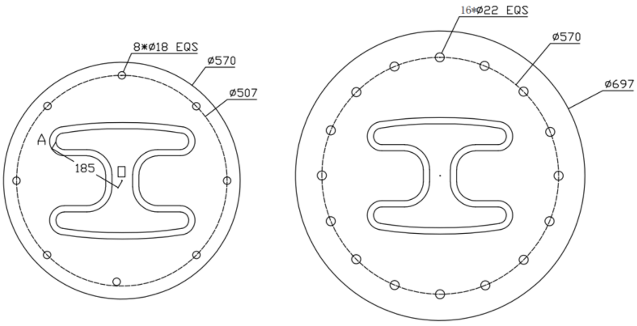

Fig 4. I-shaped upper and lower flanges.

In the solid mechanics physics field, a fixed constraint is first applied to the domain of the lower flange, as shown in Fig. 5 (a). According to the technical requirements of ZGW6-816, a rated bending load (SCL) of 16 kN is applied to the post composite insulator. Therefore, a radial force is applied to half of the boundary of the upper flange, as shown in Fig. 5 (b). Additionally, a rated torsional load (SToL) of 10 kN·m is applied to the post composite insulator. Radial forces of equal magnitude but opposite directions are applied to the inner points of the diagonal bolt holes on the upper flange, as shown in Fig.5(c). Here, the applied forces are derived based on the relationship between torque, force, and moment arm.

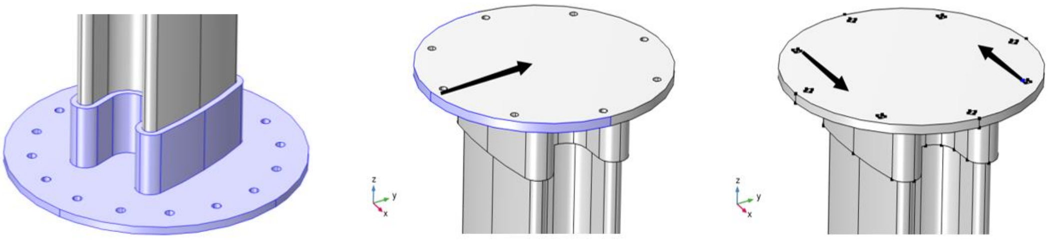

(a) fixed constraint. (b) Bending condition. (c) Torsional condition.

Fig 5. Boundary condition settings.

3. Displacement and Stress Analysis

In bending and torsion conditions, the maximum displacement and stress, as well as their distribution, were analyzed to study the deformation of the I-shaped composite post insulator.

3.1. Bending Condition

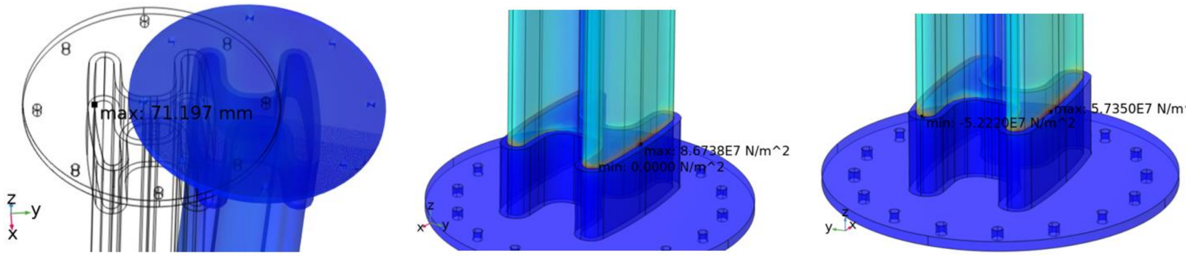

(a) Maximum Displacement Point. (b) Maximum Stress Point. (c) Maximum Normal Stress Point.

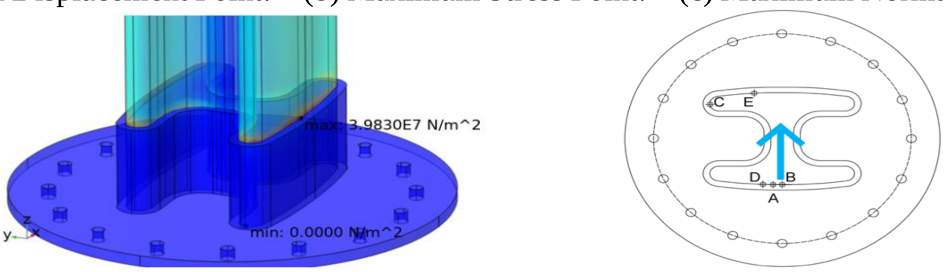

(d) Maximum Shear Stress Point. (e) Key Point Diagram.

Fig 6. Key stress and displacement points under bending condition.

From Fig. 6 (a-d), it can be seen that when a 16 kN force is applied in the y-direction at the upper flange boundary, the I-shaped pillar composite insulator undergoes bending deformation. The maximum displacement is 71.197 mm, located at the top of the core, as shown at point A in Fig. 6 (e). The maximum stress is 86.738 MPa, occurring at the midpoint of the outer bending side of the lower flange fixed constraint, as shown at point B. The maximum normal stress in the direction toward the cross-section is 57.35 MPa, located 4 cm from the midpoint of the outer bending side of the lower flange fixed constraint, as shown at point D. The maximum normal stress in the direction away from the cross-section is 52.22 MPa, located at the midpoint of the arc at the corners of the flange of the lower flange fixed constraint, as shown at point C. The maximum shear stress is 39.83 MPa, also located at point A.

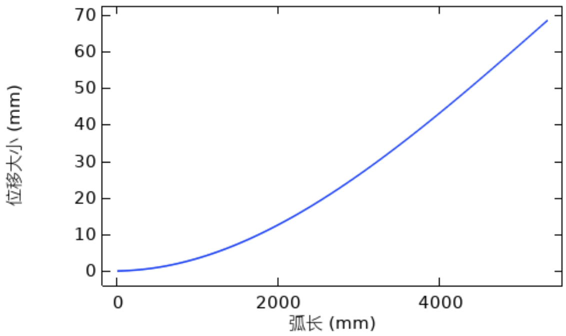

(a) Surface axial arc length-displacement distribution.

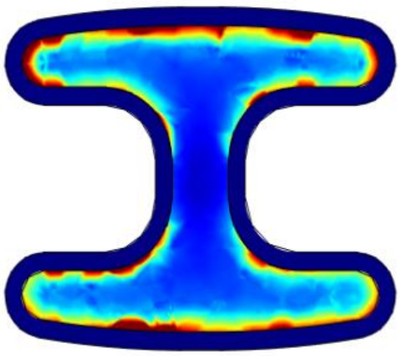

(b) stress distribution at the top cross-section (Force Applied to the Flange).

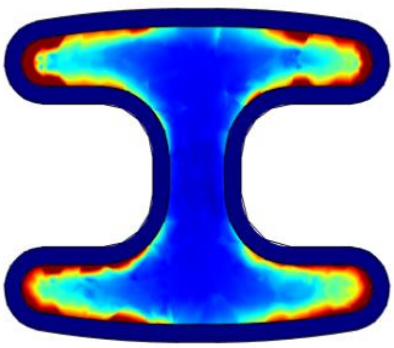

(c) Stress distribution at the top cross-section (Force Applied to the Web).

Fig 7. Displacement and stress distribution under bending condition.

From Fig.7, it can be observed that displacement increases with arc length, and the slope gradually increases. Stress is mainly distributed at the edges of the flange in the top cross-section of the lower flange, with the stress in the straight part of the web being less than that in the flange.

The following conclusions can be drawn:(1) Displacement increases toward the top, max at 71.197 mm; (2) Tensile stress is highest on the outer bending side; compressive stress is highest on the lateral side (compression < tension); (3) Shear stress is highest near the inner bending surface on the lateral side. Consider both inner/outer and lateral sides; (4) Stress is concentrated on inner/outer surfaces and high-curvature areas. Reduce curvature to improve resistance; (5) When force is applied to the web, stress concentrates at flange corners (simulation-confirmed); (6) same conclusions apply when force is applied to the web; further details omitted.

3.2. Torsion Condition

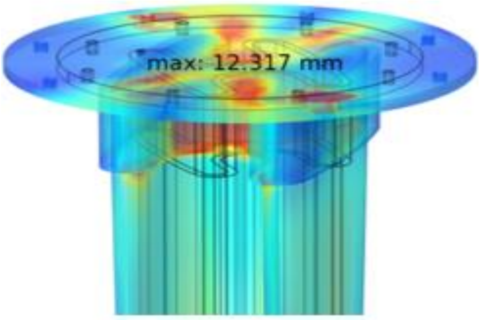

(a) maximum displacement point.

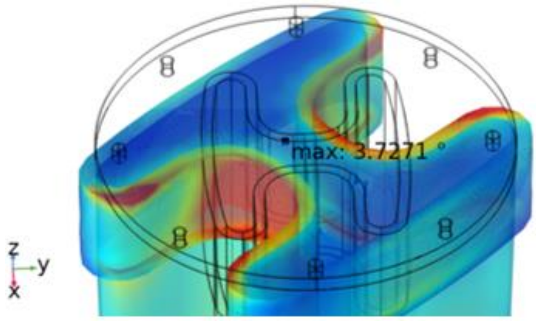

(b) maximum torsion angle point

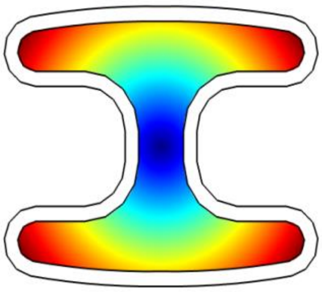

(c) 2D displacement distribution at the top surface.

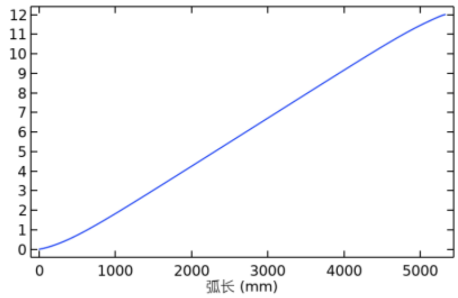

(d) height-displacement curve.

Fig 8. Displacement and Torsion Angle under Torsion Condition.

From Fig.8, it can be observed that the I-shaped pillar composite insulator undergoes torsional deformation. The maximum displacement is 12.317 mm, located at the top of the core and the outer quarter of the flange arc, as shown at point A in Fig.7. The maximum torsion angle is calculated to be 3.7271°, located at point F. Displacement increases with the distance from the center point, showing a concentric circular distribution. Therefore, point A is the farthest from the center point, and both displacement and torsion angle increase with the height of the point.

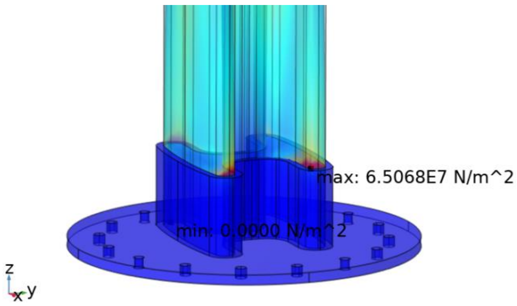

(a) Maximum Stress Point.

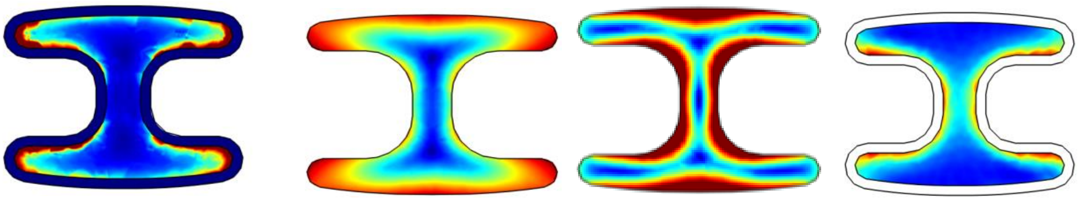

Z=160mm. Z=300mm. Z=3000. z=5630.

(b) 2D Stress Distribution Diagrams at Different Cross-Sections.

Fig 9. Stress under torsion condition.

From Fig.9, the maximum stress is 65.068 MPa, located at the inner quarter of the flange arc near the fixed constraint, as shown at point B. At the Z=160 mm cross-section, stress is mainly concentrated at the corners of the flange. At the Z=300 mm cross-section, stress is concentrated at the corners and outer edges of the flange. At the Z=3000 mm cross-section, stress is mainly distributed at the outer edges of the flange and the web side. At the Z=5630 mm cross-section, stress is primarily concentrated at the web and inner edges of the flange.

The following conclusions can be drawn: (1) Displacement and torsion angle increase with height and distance from the center, showing a concentric circular distribution. (2) Stress shifts from the flange corners to the web and inner edges as displacement increases. (3) Highest at the inner flange edges: outer edges experience tension, inner edges experience compression. (4) Concentrated at the web and inner flange edges, indicating significant slippage in the I-section's concave areas. (5) All parts of the I-shaped cross-section face concentrated stress under torsion conditions.

4. Summary

During bending, stress is concentrated on the inner and outer bending surfaces as well as areas with high curvature. Additionally, when the external force is applied to the web side, the stress is greater compared to when it is applied to the flange side. During torsion, the stress concentration points vary across different cross-sections, and all parts of the structure face challenges from concentrated stress.

References

[1] Fan Zhong, Chen Yuchen, Chai Huijuan, et al. Study on Mechanical Performance of I-Section Steel Tube Columns in Xiong'an Station. Building Structure, 2021, 51(24): 26-34.

[2] Deng Xisheng, Dong Shi'er, He Dongsheng. Optimal Design of Double-Symmetrical I-Section Beams Based on ANSYS Technology. Steel Construction, 2007(01): 34-36.

[3] Zhang Ruguang. Discussion on the Design of Large FRP Pultruded Profiles //Proceedings of the 12th Annual Conference on FRP/Composites, 1997: 103-106.

[4] Zhou Songsong, Du Yijun, Wang Xi, Deng Yu, Liu Hechen. Application Status and Issues of Epoxy Resin-Based Composites for Outdoor Composite Insulators in China. China Standardization, 2021(S1): 222-228.

[5] Wu Weining, Wu Guangya, Zhang Qin, Zhang Rui. Application and Operational Characteristics of 1000 kV UHV AC Insulators. High Voltage Engineering, 2011, 37(01): 15-20.

[6] He Faliang. Development of Large-Core Crimped Post Composite Insulators. Insulators and Surge Arresters, 2020(02): 222-228.

[7] Zhang Rui, Wu Guangya, Yuan Tian, Yao Tao, Zhang Qin, Xu Tao. Development and Prospects of Key Manufacturing Technologies for Composite Insulators in China. High Voltage Engineering, 2007(01): 106-110.